Supplementary Information

Determination of X-ray detection limit and application in perovskite X-ray detectors

Lei Pan[1], Shreetu Shrestha[2], Neil Taylor[1], Wanyi Nie[2] and Lei R. Cao[1*]

[1]*Nuclear Engineering Program, Department of Mechanical and Aerospace Engineering, The Ohio State University, Columbus, Ohio, 43210, USA*

[2]*Center for Integrated Nanotechnology Materials Physics and Application Division, Los Alamos National Laboratory, Los Alamos, NM, 87545, USA*

*Correspondence to: cao.152@osu.edu

Table S1. $MAPbI_3$ device dimensions

	#1 Au/Au	#2 Pb/Au	#3 Pb/Au	#4 Pb/Au
$MAPbI_3$ thickness (mm)	1.0	1.3	0.6	0.9
Electrode area (mm^2)	9.28	4.68	10.50	6.82
Electrode thickness (nm)	100	100	100	100

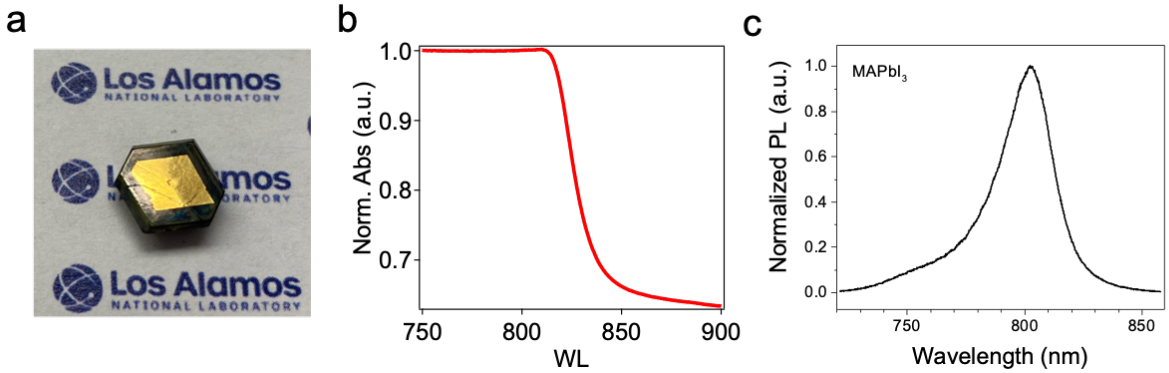

Figure S1. $MAPbI_3$ Single crystal characterizations. a. photo of a typical single crystal device. **b.** absorption spectrum and **c.** photoluminescence spectrum for $MAPbI_3$ single crystal.

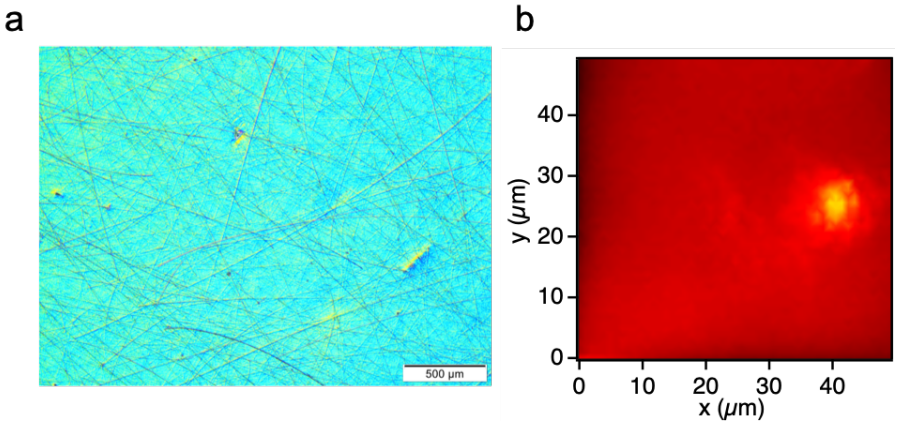

Figure S2. Surface characterizations for the $MAPbI_3$ single crystal. a. optical microscope image for $MAPbI_3$ single crystal's surface after polishing. **b.** photoluminescence height map for a typical crystal after polishing.

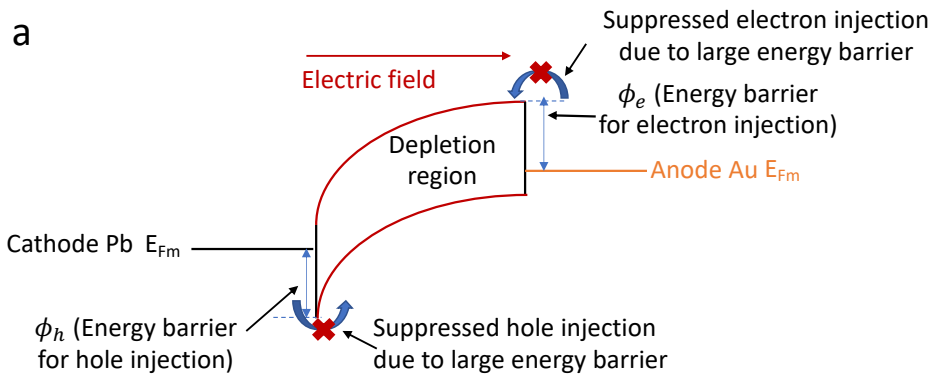

Energy band diagram of Pb/p-type $MAPbI_3$/Au at reverse bias mode
(E_{Fm}: metal Fermi level)

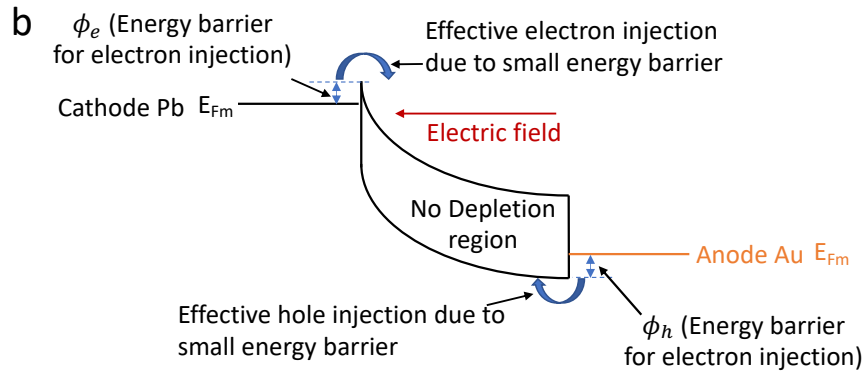

Energy band diagram of Pb/p-type $MAPbI_3$/Au at forward bias mode

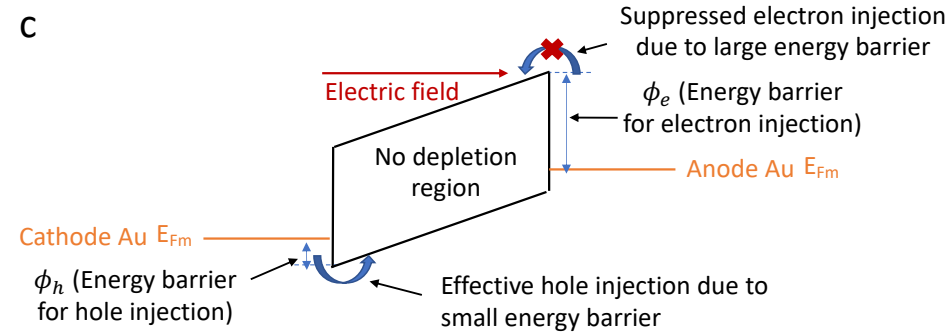

Energy band diagram of Au/p-type $MAPbI_3$/Au

Figure S3. Energy band diagram of different device architectures for charge injection analysis. a. Pb/p-type $MAPbI_3$/Au at reverse bias. **b.** Pb/p-type $MAPbI_3$/Au at forward bias. **c.** Au/p-type $MAPbI_3$/Au

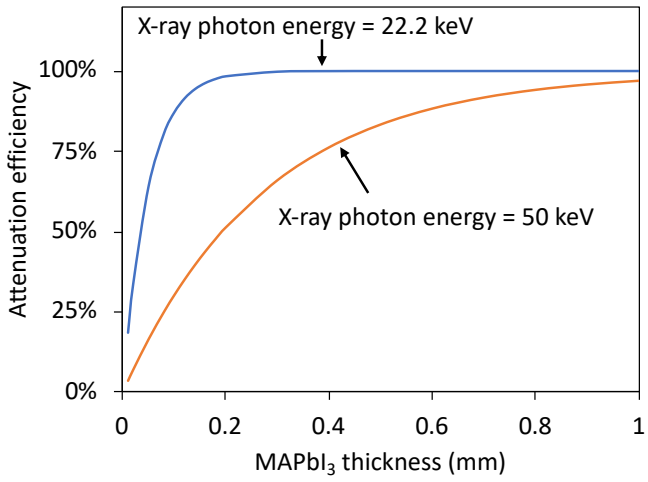

Figure S4. X-ray photon attenuation in $MAPbI_3$ signal crystal.

Attenuation efficiency = 1 - $e^{-(\frac{\mu}{\rho})\rho x}$, where $\frac{\mu}{\rho}$ is the mass attenuation coefficient of $MAPbI_3$, ρ is the density of $MAPbI_3$, and x is the $MAPbI_3$ single crystal thickness. The mass attenuation coefficient of $MAPbI_3$ can be calculated as $(\frac{\mu}{\rho})_{MAPbI3} = \sum_i w_i (\frac{\mu}{\rho})_i$ where w_i and $(\frac{\mu}{\rho})_i$ are the fraction by weight and the mass attenuation coefficient of the i^{th} atomic constituent, respectively.

The attenuation efficiencies of $MAPbI_3$ to two X-ray photon energies are calculated. The 22.2 keV and 50 keV are the most probable energy and the maximum energy, respectively, of the X-ray tube used in this work (see **Figure S8**). It can be effectively treated that the charge carriers are generated at the surface of the $MAPbI_3$ single crystal due to the limited penetration depth of the X-ray photons, *i.e.*, less than 0.2 mm for 22.2 keV X-ray photons.

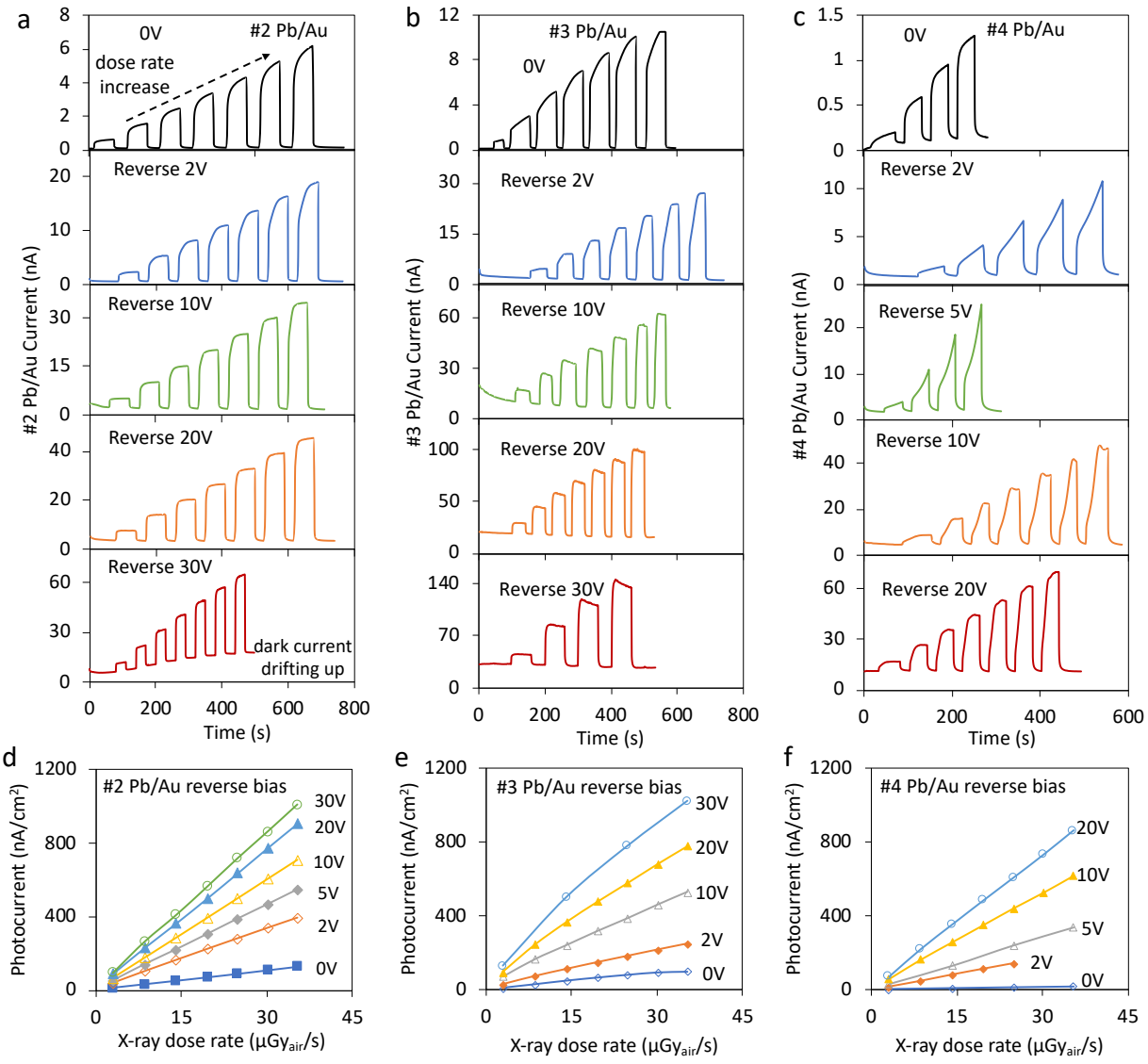

Figure S5. Sensitivity measurement of reversely biased Pb/Au devices at charge collection mode. Current response (hole-dominantly induced signal) of **a.** #2 Pb/Au device, **b.** #3 Pb/Au device **c.** #4 Pb/Au device, to increased X-ray dose rate in air at different reverse voltage. Photocurrent density as function of X-ray dose rate in air of **d.** #2 Pb/Au device, **e.** #3 Pb/Au device **f.** #4 Pb/Au device, at different reverse voltage.

Photocurrent is calculated as the difference between the signal current when X-ray is turned on and the dark current. sensitivity is obtained as the slope of linear fitting to photocurrent density as function of X-ray dose rate in air.

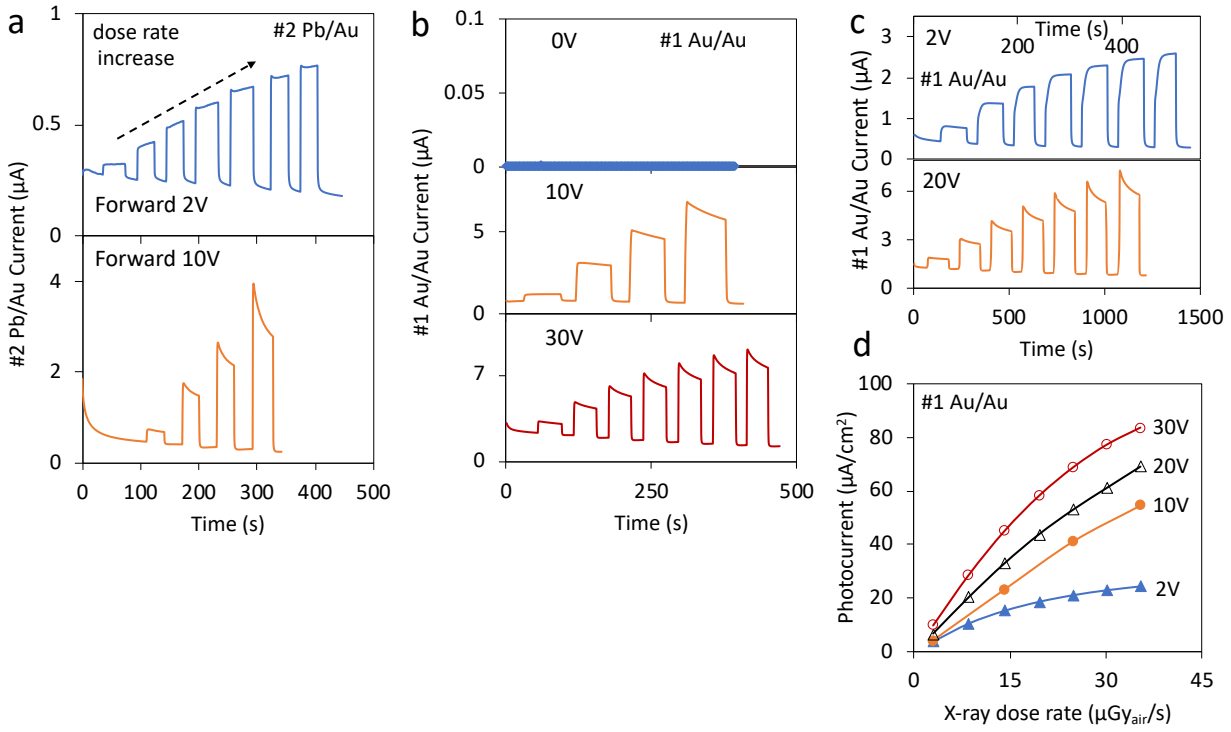

Figure S6. Sensitivity measurement of forward biased Pb/Au devices and Au/Au device at charge injection mode. Current response (hole-dominantly induced signal) of **a.** forward biased #2 Pb/Au device, **b. c.** #1 Au/Au device, to increased X-ray dose rate in air at different voltage. **d.** Photocurrent density as function of X-ray dose rate in air of #1 Au/Au device.

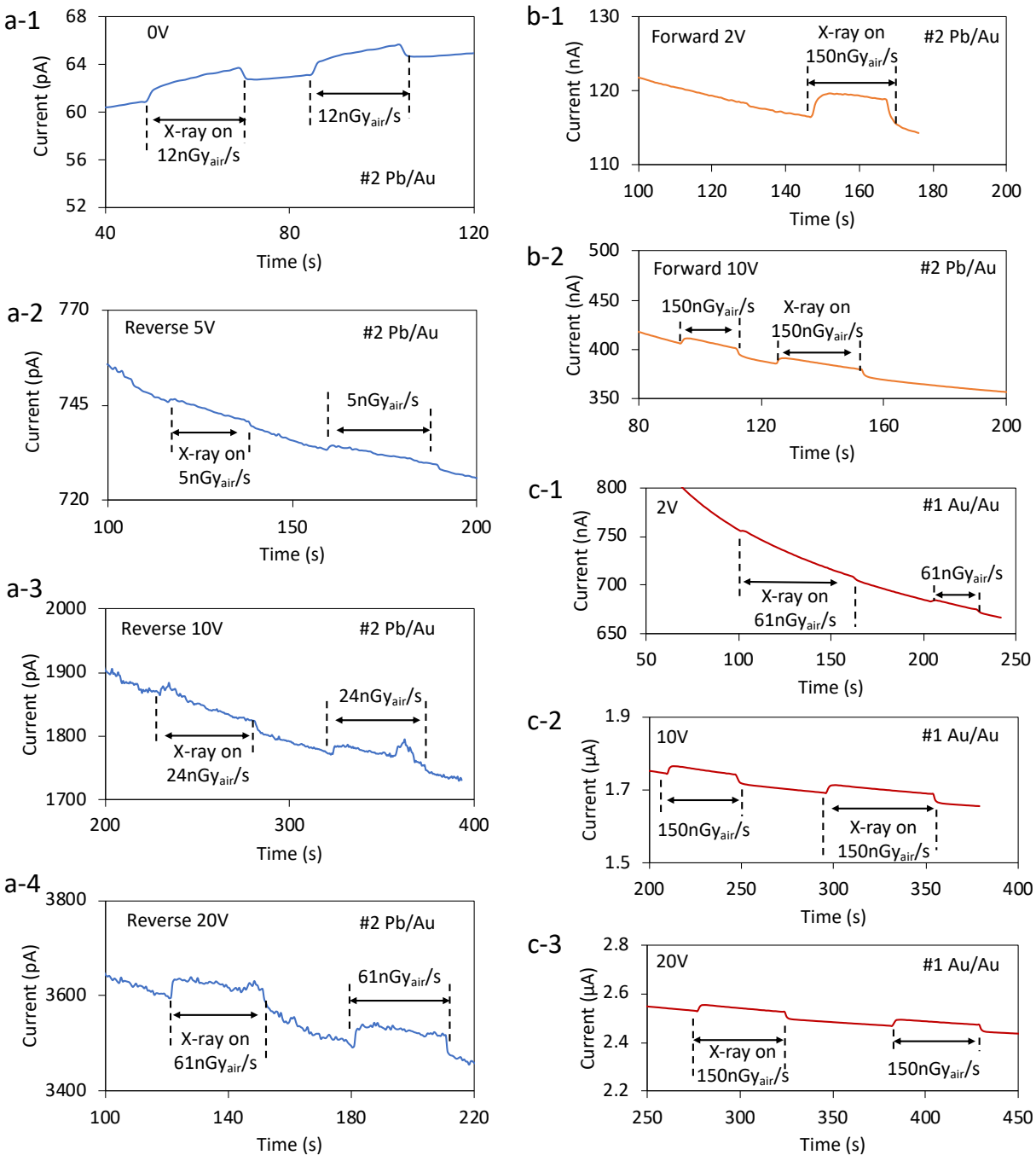

Figure S7. *Posterior* check of the detectability. a. Current response of reversely biased #2 Pb/Au device at different reverse voltage. The X-ray dose rate shown in the figures are confirmed to be detected by *posterior* check method, which supports the *prior* calculated detection limit. **b.** Current response of forward biased #2 Pb/Au device at different forward voltage. **c.** Current response of #1 Au/Au device at different voltage.

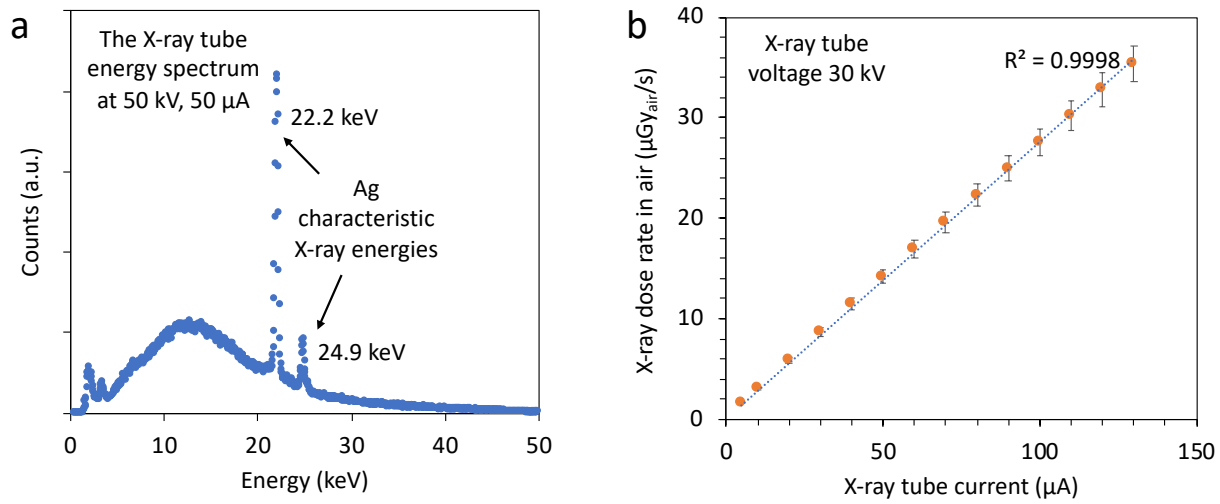

Figure S8. X-ray tube (with Ag target) energy spectrum and dose rate calibration a. X-ray tube energy spectrum at tube voltage 50 kV and tube current of 50 µA, measured by a Si P-I-N detector. **b.** X-ray tube dose rate in air at tube voltage 30 kV and different tube current from 5 µA to 130 µA. A dosimeter (Fluke Biomedical RaySafe 452) was used for dose rate calibration.

The X-ray tube has a most probable X-ray photon energy of 22.2 keV, corresponding to one of the Ag characteristic X-ray energies when the X-ray tube is operated at voltage higher than 22.2 kV.

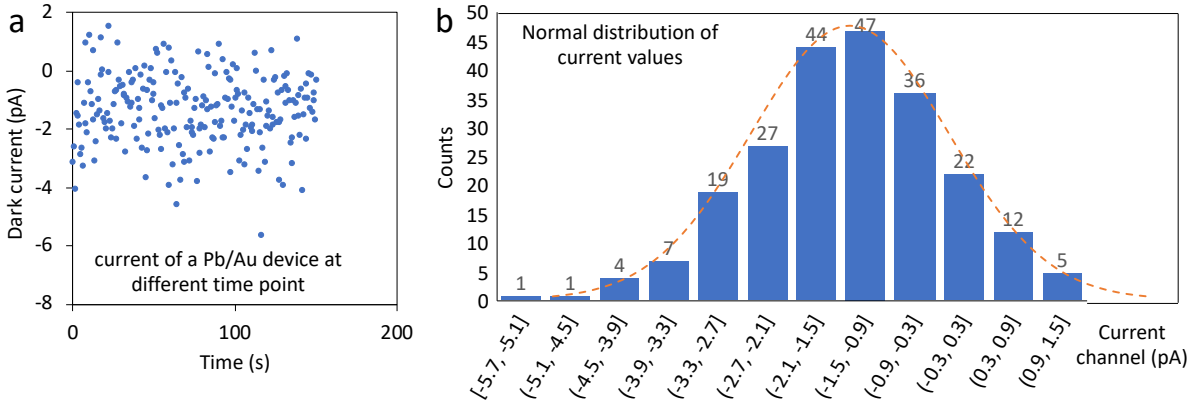

Figure S9. Statistical distribution of the current values. a. dark current of a Pb/Au device measured as a function of time. The measurement was performed at 0V to avoid the interference of dark current drift. **b.** Current value distribution fitting to Normal distribution, supporting the assumption of Normal distribution.